Numerical analysis of astigmatism correction in gradient refractive index lens based optical coherence tomography catheters

Tianshi Wang,[1,*] Antonius F. W. van der Steen,[1,2] and Gijs van Soest[1]

[1]Thorax Center, Erasmus University Medical Center, P.O. Box 2040, Rotterdam 3000CA, The Netherlands

[2]Interuniversity Cardiology Institute of The Netherlands, P.O. Box 19258, Utrecht 3051DG, The Netherlands

*Corresponding author: t.wang.1@erasmusmc.nl

Received 25 April 2012; accepted 27 May 2012;
posted 6 June 2012 (Doc. ID 167344); published 18 July 2012

Endoscopic optical coherence tomography (OCT) catheters comprise a transparent tube to separate the imaging instrument from tissues. This tube acts as a cylindrical lens, introducing astigmatism into the beam. In this report, we quantified this negative effect using optical simulations of OCT catheter devices, and discuss possible compensation strategies. For esophageal imaging, the astigmatism is aggravated by the long working distance. For intracoronary imaging, the beam quality is degraded due to the liquid imaging environment. A nearly circular beam profile can be achieved by a curved focusing optics. We also consider the method of matching refractive indices, and it is shown to successfully restore a round beam.

OCIS codes: 170.4500, 220.4830.

1. Introduction

A. Background

Optical coherence tomography (OCT) can perform noninvasive, cross-sectional imaging of biological tissue [1]. OCT is widely used in biomedical analysis and medical diagnosis, offering high-resolution (approximately 15 μm) imaging of tissue, with an image penetration depth of 1–2 mm, depending on tissue optical properties. It is commonly applied in ophthalmology for diagnosis of retinal diseases [2] and increasingly for endoscopic applications as well [3].

In endoscopic OCT for both coronary and esophageal imaging, the established methods use a guidewire or an endoscope instrumentation port to direct a catheter along into the lumen of the organ under investigation. When the catheter is positioned at the region of interest, cross-sectional images are acquired by rotary sideview scanning [4–8]. The sideview scanning can be realized by rotating the optical tip of catheter with a proximal motor. The rotating imaging element is pulled back inside the lumen under investigation to acquire a volume data set.

Two important applications of endoscopic OCT are imaging of the coronary circulation and of the upper gastrointestinal tract. Studies have shown the capability of OCT to perform screening for Barrett's esophagus, delineating gastrointestinal mucosal microstructure and distinguishing dysplastic from normal tissues [4,8]. In order to center the catheter in the relatively large lumen of the esophagus, balloon catheters have been developed to enable reproducible circumferential scanning.

The first *in vivo* demonstration of intracoronary OCT imaging in human was performed in 2001, demonstrating diagnostic imaging of arterial wall pathologies and coronary interventions [9]. Since then, the technology has become commercially available. It is primarily used for inspection of stents and for diagnosing unstable forms of coronary

1559-128X/12/215244-09$15.00/0

atherosclerosis [10–15]. For intravascular imaging, the primary challenge is to clear the strongly scattering red blood cells. An efficient clinical solution is to displace the blood temporarily by flushing the artery with saline or x-ray contrast dye [5,11,12,16,17].

OCT depends on a spatially coherent wavefront, the shape of which determines the point spread function. Image quality, in terms of contrast and resolution, benefits from a well-characterized, round beam shape. In endoscopic applications in particular, controlling the wavefront can be a challenge because of the limited space available for the optics in the probe. In this study, we characterize the effect of endoscope optical design and discuss strategies for optimization of the beam characteristics for imaging.

B. Astigmatism Introduced by the Catheter Outer Tube

A transparent protective tube is commonly applied on the outside of the catheter. This tube isolates the tissues under investigation from rotating catheter parts, guides the pullback motion, and protects the catheter inside from blood and mechanical damage. However, while effectively separating tissue and device, the tube acts as a negative cylindrical (concave/convex) lens, contributing to divergence of the light beam in one direction [18–22]. As illustrated in Fig. 1, the beam waists are different in vertical and horizontal direction of light beam, and are found at different locations: the beam becomes astigmatic. The extra divergence will lead to a decrease in transverse resolution, image contrast, and Strehl ratio [18–20]. A long working distance (distance from focal point to optical axis of the device), as is required for esophageal imaging, or a liquid environment, as in intracoronary imaging, aggravate the problem. In these cases, the additional divergence should be taken into consideration for catheter design.

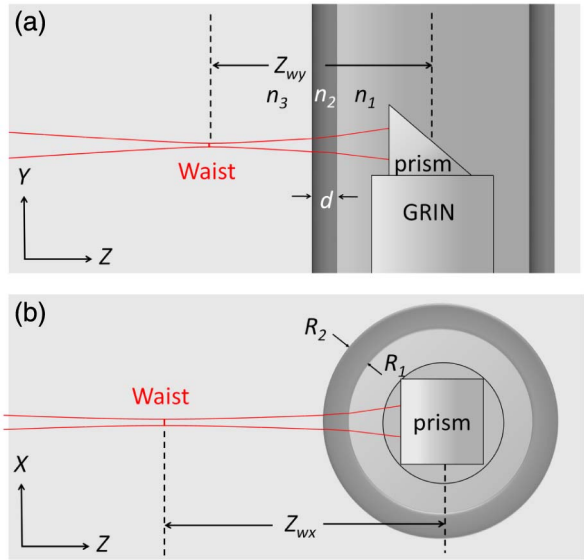

Fig. 1. (Color online) Schematic diagram of imaging catheter tip, shown in (a) side view; (b) top view. n_1: index of inner medium, n_2: index of tube, n_3: index of outer medium, R_1: inner radius of tube, R_2: outer radius of tube, d: thickness of tube, z_w: working distance (z_{wx} in azimuthal direction, z_{wy} in longitudinal direction).

The astigmatism of the beam (and the resulting point spread function) is not necessarily evident from the acquired data. Particularly in coronary imaging, the artery under investigation is routinely sampled with a frame pitch of 200 μm, much larger than the spot size in either direction. The imaged volume is grossly undersampled in the pullback direction.

In previous studies, Xi *et al.* [20] and Kang *et al.* [21] described a correction method for long working distance endoscopes, to refocus the light beam along one direction with a cylindrical mirror or prism to approach a circular beam profile. Swanson *et al.* [23] provided another method based on matching the refractive index for imaging in a fluid environment.

In the present paper, we will quantify the astigmatism based on optical simulations and provide a systematic way to optimize the beam compensation in different catheter types.

2. Methods

A. Probe Optical Design and Geometry

The common optical design, widely applied in both esophageal and coronary OCT imaging, is to focus the Gaussian beam emitted from a single mode fiber (SMF) using a gradient refractive index (GRIN) lens [7,17,20,21,23–26].

In our simulations, we assume the imaging beam is perpendicular to the catheter, neglecting the small offset angle that is usually chosen to reduce sheath reflections. We will adopt the following terminology for the beam parameter coordinates (see also Fig. 1). The spot is described in the cross-section (x, y) plane perpendicular to the direction of beam (z). The x-axis of the plane is chosen in the image plane, perpendicular to catheter, and is called the "azimuthal" direction, as it coincides with the rotation direction of the catheter. The y-axis is parallel to the catheter, and is called the "longitudinal" direction, as this is the pullback direction, and the longitudinal direction of the luminal organ under investigation.

The enclosing transparent tube is commonly made of flexible optical transparent plastic, such as fluorinated ethylene propylene (FEP) or polyethylene (PE). As illustrated in Fig. 1, the light beam defocuses in the x-z plane as a common negative effect in almost all sideview OCT probes. The ray transfer matrixes of the tube are shown as follows in two directions, respectively:

In the x-z (image) plane,

$$\begin{pmatrix} 1 & 0 \\ \frac{n_2-n_3}{R_2 n_3} & \frac{n_2}{n_3} \end{pmatrix} \begin{pmatrix} 1 & d \\ 0 & 1 \end{pmatrix} \begin{pmatrix} 1 & 0 \\ \frac{n_1-n_2}{R_1 n_2} & \frac{n_1}{n_2} \end{pmatrix} = \begin{pmatrix} 1 + d\frac{n_1-n_2}{R_1 n_2} & \frac{dn_1}{n_2} \\ \frac{n_2-n_3}{R_2 n_3} + \frac{d(n_2-n_3)(n_1-n_2)}{R_1 R_2 n_2 n_3} + \frac{n_1-n_2}{R_1 n_3} & \frac{n_1}{n_3} + \frac{dn_1(n_2-n_3)}{n_2 n_3 R_2} \end{pmatrix}. \quad (1)$$

In the y-z plane (containing the catheter),

$$\begin{pmatrix} 1 & 0 \\ 0 & \frac{n_2}{n_3} \end{pmatrix}\begin{pmatrix} 1 & d \\ 0 & 1 \end{pmatrix}\begin{pmatrix} 1 & 0 \\ 0 & \frac{n_1}{n_2} \end{pmatrix} = \begin{pmatrix} 1 & \frac{dn_1}{n_2} \\ 0 & \frac{n_1}{n_3} \end{pmatrix}. \quad (2)$$

The resultant working distance z_w and beam waist w_0 will be calculated in x and y directions; designated by appropriate subscripts.

B. Simulation

In order to simulate the astigmatism effect and the compensation methods, we applied a model of a GRIN lens–based catheter including commercially available GRIN lens ($g = 1.372\ \text{mm}^{-1}$ and $0.636\ \text{mm}^{-1}$) and a glass spacer, single-mode fiber (mode field diameter $= 9.2\ \mu$m at 1310 nm wavelength), a plastic tube, and a reflect mirror (or a prism). The parameters of the GRIN lens and glass spacer are first calculated by paraxial Gaussian beam analysis. The Gaussian beam can be characterized by two parameters: the beam waist (w_0) and the distance from reference plane to beam waist, which can be expressed by the complex beam parameter q [27]:

$$q_1 = Z + Z_R i = Z + \frac{\pi n_m w_0^2}{\lambda} i, \quad (3)$$

where Z denotes the distance from the beam waist to the reference plane; Z_R is the Rayleigh length; w_0, the beam waist; λ, the wavelength; and n_m is the refractive index of the propagation medium. An optical system can be characterized by the ray transfer matrix (ABCD matrix). The Gaussian beam, defined at the entrance by q_l, is transformed by the optical system as [27]:

$$q_2 = \frac{Aq_1 + B}{Cq_1 + D}. \quad (4)$$

If the ray transfer matrix is known, one can adjust the parameters of output Gaussian beam in focal length and beam waist by manipulating the elements of the ABCD matrix. The equivalent ABCD matrix describing the propagation of a Gaussian beam in a GRIN lens is given by [28]:

$$\begin{pmatrix} A & B \\ C & D \end{pmatrix} = \begin{pmatrix} 1 & f \\ 0 & 1 \end{pmatrix}\begin{pmatrix} 1 & 0 \\ 0 & \frac{n_g}{n_m} \end{pmatrix}\begin{pmatrix} \cos(gl_g) & \frac{\sin(gl_g)}{g} \\ -g\sin(gl_g) & \cos(gl_g) \end{pmatrix} \times \begin{pmatrix} 1 & 0 \\ 0 & \frac{n_s}{n_g} \end{pmatrix}\begin{pmatrix} 1 & l_s \\ 0 & 1 \end{pmatrix}\begin{pmatrix} 1 & 0 \\ 0 & \frac{n_f}{n_s} \end{pmatrix}. \quad (5)$$

Here, n_f is the refractive index of the fiber, n_g denotes the axial refractive index of GRIN lens, l_g is the length of the GRIN lens, g is the gradient constant of the GRIN lens, n_s is the refractive index of the spacer, l_s is the length of the spacer, and f is the focal length of the lens.

The focal length (f) and beam waist (w_0) of the output beam can be related to the GRIN lens and spacer parameters, and the mode field radius of the single-mode fiber (w_s) [26]. These relations can be solved for l_g and l_s to yield the optimal lengths of the GRIN lens and spacer given the desired focal length and beam waist for a specific application. The parameters, calculated based on the paraxial Gaussian matrix transformation, will be further optimized by physical optics formalism as implemented in Zemax 2008 (ZEMAX Development Corp.) to obtain a better approximation. We quantify the astigmatism by the spot ellipticity of the output beam. In particular, the optical surfaces that are not collinear with the optical axis cannot be accurately modeled using the Gaussian paraxial approximation. The compensation performed on the esophageal and coronary imaging simulation models will also be evaluated by applying the physical optics formalism for better approximation.

C. Catheter Model for Esophageal Imaging

The balloon used for esophageal imaging commonly has a diameter of 20 mm. Consequently, most of the published balloon catheter designs have a working distance of 9–12 mm. Spot sizes range from 15–40 μm. The properties of output light beam are mainly related to the maximum beam diameter (MBD) within the GRIN lens. A long working distance requires long focal length, which means the MBD needs to be expanded to maintain a small beam waist. This can be achieved in different ways: one is to expand the input spot size at the GRIN lens by increasing the spacer length l_s [25]. Another is to increase the divergence of the input beam by decreasing its waist, which can be realized by applying another GRIN lens between SMF and spacer [20,26]. While expanding the beam within the GRIN lens, the MBD should be limited to 80% of the lens aperture to ensure the beam profile remains Gaussian. In our simulation model, we applied a model of a single GRIN lens probe as shown in Fig. 2. The light beam, coming from an SMF28 fiber, is expanded by a 3.7 mm length glass spacer ($n_s = 1.5$) before entering a 0.7 mm length, 1.0 mm diameter GRIN lens ($g = 0.636\ \text{mm}^{-1}$). A mirror is at 2 mm distance from the GRIN lens, and deflects the light beam to an FEP tube ($R_1 = 0.75$ mm, $d = 0.1$ mm). The simulation shows that the ideal working distance $z_w = 11.25$ mm and forms a waist of 23.1 μm.

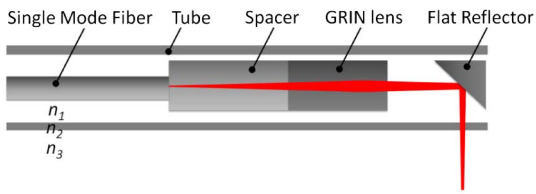

Fig. 2. (Color online) Schematic diagram of the simulation model of a GRIN lens–based OCT probe with a reflector;n_1: index of inner medium, n_2: index of tube, n_3: index of outer medium.

D. Catheter Model for Coronary Imaging

For cross-sectional visualization of the entire coronary artery (diameter: 3–4 mm) with sufficient resolution, a relatively short working distance (approximately 1–2 mm) and long depth of field (preferably preferably > 2 mm) are necessary, albeit at the cost of increasing the beam waist, which is commonly 20–30 μm [11,23]. In practice, the outer diameter of a coronary imaging catheter is limited to 1 mm or slightly more, including the protective tube [17,23].

In our work, we applied a probe model, as shown in Fig. 3, which is a typical design based on a GRIN lens. A high gradient constant GRIN lens ($g = 1.372\ \mathrm{mm}^{-1}$) attached to a prism is used to shorten the length of rigid part. Parameters were set as: GRIN lens (diameter $= 0.50$ mm, $l_g = 1.10$ mm, $g = 1.372\ \mathrm{mm}^{-1}$), Glass spacer (diameter $= 0.50$ mm, $l_s = 0.14$ mm, $n_s = 1.50$). Microprism ($n = 1.50$, length of short side $= 0.35$ mm), FEP Tube ($R_1 = 0.40$ mm, $d = 0.10$ mm). The simulation shows that the ideal light beam attains a focus at $z_w = 1.46$ mm and forms a 20.8 μm beam waist.

For coronary imaging, the optics of the OCT beam will be affected by the refractive index of the flush medium in the artery, which is used to displace the blood. The specific media that are commonly used, and that we will also use in this paper, are saline ($n_3 = 1.33$) and the contrast dye Iodixanol 370 (Visipaque, GE Healthcare; $n_3 = 1.45$).

E. Minimization of the Astigmatism

For optimal image quality, the beam shape should be as round as possible along the light path, which means the beam parameters in azimuthal and longitudinal directions should be equalized by correcting the working distance and beam waist in the azimuthal direction, targeting those in the longitudinal plane. Ideally, the compensation for laser astigmatism can be realized by a pair of interfaces such as cylindrical lens or an anamorphic prism. Two curved surfaces are needed in general, because both the beam size and the divergence need to be compensated, and these parameters are not independent if only one cylindrical surface is applied.

We compute the optimal compensation by setting the beam parameters at the focus to the desired ones and backpropagating the beam through the tube and the catheter optics to compare both beam directions at a reference surface. The compensation is simulated in the azimuthal direction, aiming to refocus the light beam back to the target focal point, and adjusting the radius of curvature R_c of the correcting surface to achieve optimal focusing. The optimization is performed on the spot deviation, which is the absolute value of difference between spot ratio and 1, integrated over the Rayleigh range:

$$\Delta_w = \int_{z_w - z_R}^{z_w + z_R} |w_x(z)/w_y(z) - 1| \mathrm{d}z, \tag{6}$$

where z_w is the target working distance, z_R is the Rayleigh length, and $w_x(z)$ and $w_y(z)$ are the spot sizes with distance z from the optical axis, respectively in the azimuthal and longitudinal directions. The beam is optimized when this integral is minimized.

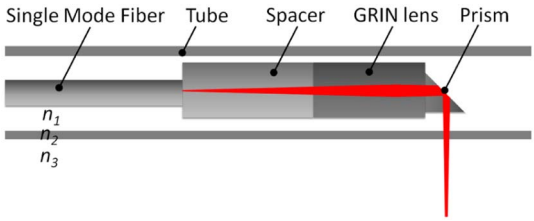

Fig. 3. (Color online) Schematic diagram of simulation mode for a GRIN lens–based OCT probe with a prism;n_1: index of inner medium, n_2: index of tube, n_3: index of outer medium.

3. Results

A. Characterization of Astigmatism

In order to characterize the astigmatism introduced by the tube, we calculated the spot size at the target focal plane in the azimuthal direction, with different parameters based on paraxial Gaussian formalism, including tube material and dimensions, and design the working distance of the light beam. Calculations were performed with air as outer and inner media.

The results are shown in Fig. 4. A thick-walled tube made of high-index material, such as polyethylene (PE), causes stronger astigmatism. Use of a thin-walled tube, made of low-index material, minimizes astigmatism; under these conditions, the ray transfer matrices approach the same limit in two directions. For a short working distance probe, the effect is well controlled in this manner; for instance: for $R_1 = 0.5$ mm, with $d = 0.05$ mm, $z_w = 2$ mm, and $w_0 = 20$ μm, the spot size at the target focal plane will be $w_x = 22.2$ μm in the azimuthal direction after an FEP tube is applied. In contrast, the spot size expands quickly with increasing thickness of the tube, particularly for long working distance probes.

The application of endoscopic catheters in a liquid environment further aggravates the astigmatism. As shown in Fig. 5, the spot size in the azimuthal direction increases quickly with increasing index of the outer medium.

B. Astigmatism of Esophageal Imaging Catheters

The long working distance results in a relatively large spot size on the tube wall, which enhances the defocusing effect of the cylindrical tube. Figure 6 shows the astigmatic beam and the spot profile at the target focal plane. This design achieves $z_{wy} = 11.25$ mm and $w_{0y} = 23.1$ μm in the longitudinal direction. Due to the defocusing effect of the tube, the working distance in the azimuthal direction will be shifted to $z_{wx} = 19.95$ mm, forming a waist w_{0x} of 41.7 μm. At the target focal plane, the spot size in the azimuthal direction w_x is nearly 100 μm, whereas $w_y = w_{0y} = 23.1$ μm. As the spot expands, the energy of the spot spreads from center to periphery, which

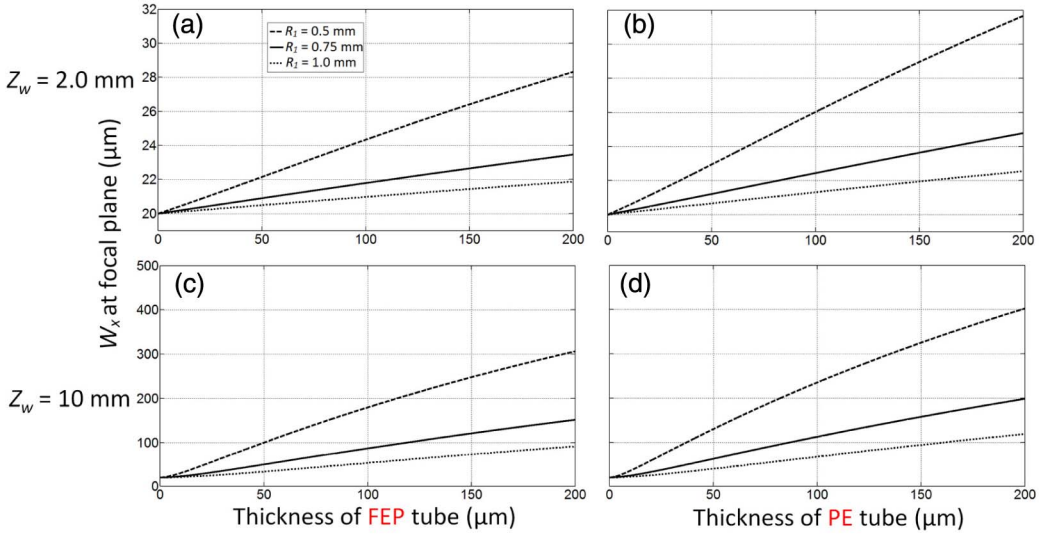

Fig. 4. (Color online) Dependence of the spot size at the target focal plane in the azimuthal direction on the thickness of the tube for different inner radius (R_1). (a) and (b): Short working distance ($z_w = 2.0$ mm); (c) and (d): long working distance ($z_w = 10$ mm). (a) and (c): Fluorinated ethylene propylene (FEP) tube ($n_2 = 1.34$); (b) and (d): polyethylene (PE) tube ($n_2 = 1.50$). The beam waist was set to be $w_0 = 20$ μm; $n_1 = n_3 = 1.0$.

reduces the irradiance peak value by a factor of 3. Lower irradiance peak value will reduce the magnitude of the impulse response (point spread function) in the lateral direction, and thus lead to degradation in image contrast.

C. Optimal Compensation for Esophageal Imaging Catheters

The backpropagated spot size in the azimuthal direction inside the tube is shown in Fig. 7, compared to the desired beam dimension. The azimuthal spot size of the light beam is close to the desired spot size within the tube and is identical to the desired one at plane A. At this location, the compensation can be achieved to a good approximation with single cylindrical interface, using a cylindrical mirror or cylindrical lens to correct the divergence; spot size correction is not needed here [29]. Conversely, at plane B, both diameter and divergence of the beam need to be corrected and two cylindrical surfaces are required.

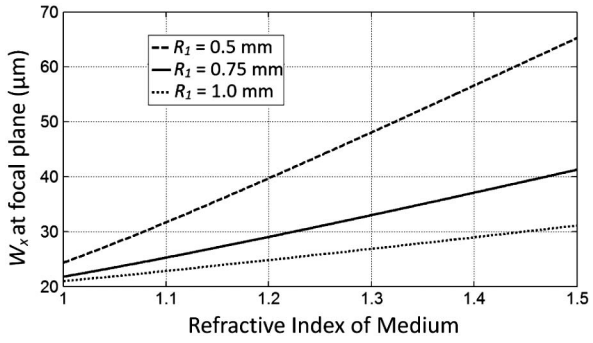

Fig. 5. Plot of spot size at focal plane in azimuthal direction versus refractive index of medium with various inner radius (R_1) of tube, made of 0.1 mm thickness FEP ($n = 1.34$). $z_w = 2.0$ mm; $w_0 = 20$ μm.

Figure 8 shows two compensations performed with a cylindrical mirror at plane A and a cylindrical lens at plane B, respectively. The reflector in Fig. 2 is replaced by a cylindrical one in Fig. 8(a): the cylindrical interface is applied at plane A as shown in Fig. 7(a). Alternatively, a cylindrical lens is used in Fig. 8(b) with the correcting surface located at plane B.

The compensation results are shown in Table 1. The light beam is efficiently refocused back to the target working distance, while the working distances in both directions are almost identical after compensation. A round spot shape with ellipticity $w_x/w_y = 1.00$ is achieved with cylindrical mirror compensation, whereas $w_x/w_y = 1.04$ with cylindrical lens compensation. The small remaining astigmatism when applying a cylindrical lens is due to use of only

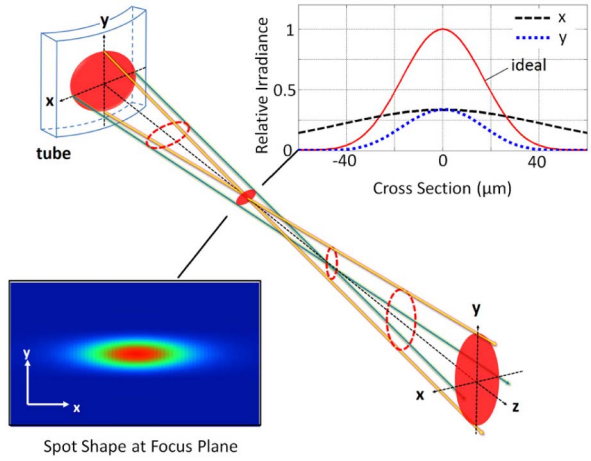

Fig. 6. (Color online) The irradiance profile of the astigmatic beam emitting from the tube with spot profile at target working distance. The scale bar is 50 μm; x: azimuthal direction, y: longitudinal direction.

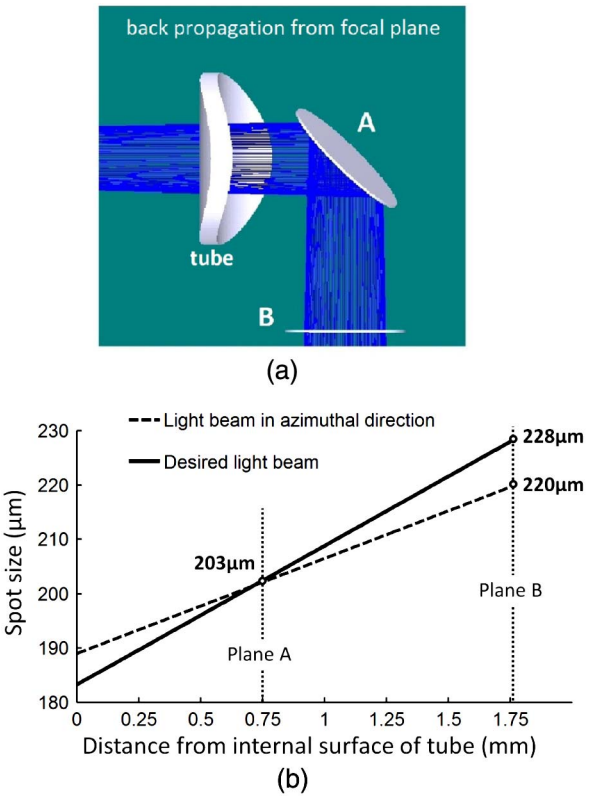

Fig. 7. (Color online) (a) Schematic of Gaussian beam inside the tube, back-propagated from the focal plane, for a long working distance catheter: the interfaces of the mirror and lens are located at plane A (the reflector) and plane B (the distal lens surface) respectively; (b) Spot sizes of the Gaussian beam in azimuthal direction and the desired light beam varying with distance from the internal surface of the tube. The distances from the tube to the compensation planes are: A, 0.75 mm; B, 1.75 mm.

Table 1. Beam Characteristics for an Esophageal Imaging Probe, and Two Compensation Methods[a]

		No compensation	Cylindrical lens	Cylindrical reflector
Working distance z_w	z_{wx} (mm)	19.95	11.25	11.25
	z_{wy} (mm)	11.25	11.25	11.25
Spot size at z_w	w_x (μm)	96.5	24.0	23.2
	w_y (μm)	23.1	23.1	23.1
Ellipticity	w_x/w_y	4.17	1.04	1.00

[a]Design working distance $z_w = 11.25$ mm; beam waist $w_0 = 23.1$ μm. Compensation parameters: cylindrical lens: BK7 glass, thickness 1.5 mm, radius of curvature $R_c = 15.5$ mm; cylindrical reflector $R_c = 35.7$ mm.

one interface for correction at plane B rather than two.

D. Astigmatism of Coronary Imaging Catheters

An intracoronary imaging catheter is immersed in fluid while imaging. The curved inner surface of the (air-filled) tube now has a significantly higher optical power than the outer surface, which is partially index-matched by the fluid surrounding the catheter, inducing strong astigmatism. Table 2 shows the dependence of the spot profile on the distance from the tube in air, saline, and Visipaque, respectively. In air, though slightly defocused, the light beam can still form a waist of $w_{0x} = 25.1$ μm waist at $z_{wx} = 1.51$ mm, versus $w_{0y} = 20.8$ μm at $z_{wy} = 1.46$ mm.

For higher refractive index of the external medium, the defocusing effect of the tube becomes progressively stronger, and finally results in a total defocusing light beam in the azimuthal direction for $n > 1.15$. The spot size in the azimuthal direction

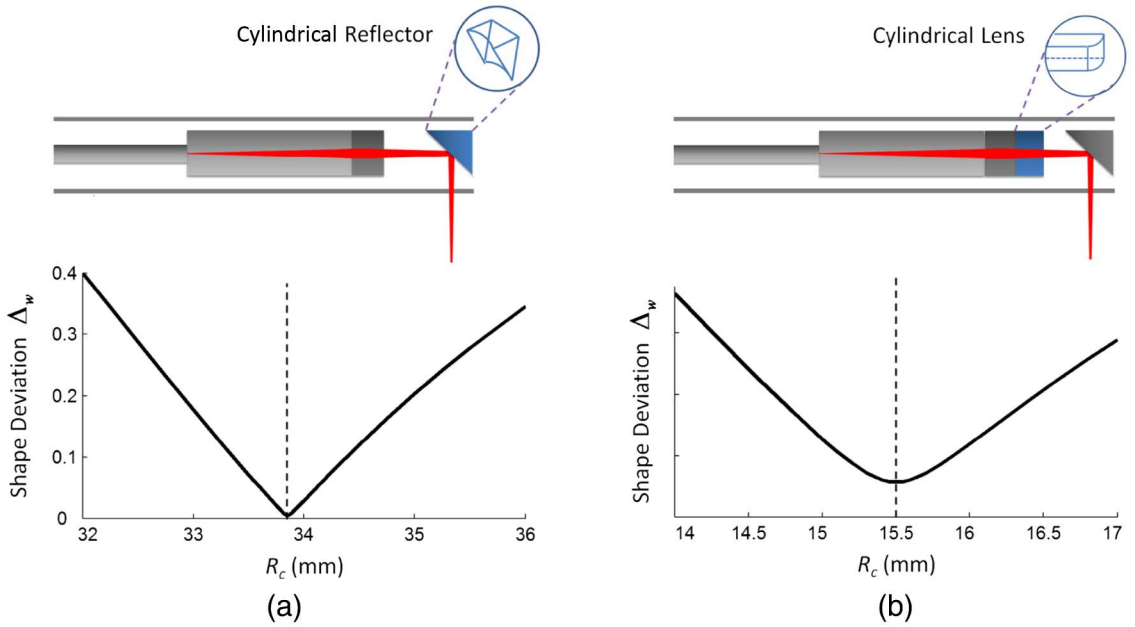

Fig. 8. (Color online) Schematic diagrams of simulation mode for a GRIN lens probe with (a) a cylindrical mirror and (b) a cylindrical lens. Near-perfect correction is achieved using a cylindrical mirror in plane A. GRIN lens diameter: 1 mm; l_g: 0.7 mm; g: 0.636 mm^{-1}; glass spacer l_s: 3.7 mm; n_s: 1.5. R_c: Curvature Radius.

Table 2. Spot Shape with Various Distances (z) from Optical Axis in Air, Saline, and Visipaque[a]

		Emitting plane	Target focal plane	Rayleigh plane
In air(index: 1.0)	z (mm)	0.50	1.46	2.50
	w_x at z (μm)	30.2	25.1	30.0
	w_y at z (μm)	28.3	20.8	29.4
	ellipticity	**1.07**	**1.21**	**1.02**
In Saline(index: 1.37)	z (mm)		1.81	3.24
	w_x at z (μm)		44.7	62.8
	w_y at z (μm)		20.8	29.4
	ellipticity		**2.15**	**2.13**
In Visipaque (index: 1.45)	z (mm)		1.89	3.39
	w_x at z (μm)		49.2	71.5
	w_y at z (μm)		20.8	29.4
	ellipticity		**2.37**	**2.43**

[a]Data in the emitting plane are independent of imaging media. The Rayleigh plane is located at the Rayleigh distance in the y-direction.

continuously expands with increasing distance, while the light beam in the longitudinal direction is focused at 1.81 mm working distance in saline, and at 1.89 mm in Visipaque, with the same beam waist as target.

E. Compensation for Coronary Imaging by a Cylindrical Interface

In order to maintain a round spot profile at the focal plane, we applied single cylindrical interface to make the compensation. The simulation is performed with a probe immersed in Visipaque. The deviation between the azimuthal spot size and the target, shown in Fig. 9, increases rapidly with distance from the internal tube surface. This situation is unlike the case of the esophageal catheter, where a plane with the desired beam profile could be identified for effective, single curvature correction.

In the intracoronary catheter, the compensation interface should be applied as close as possible to the internal surface of the tube to match the curvature. This can be approximated by replacing the emitting plane of the prism by a cylindrical one, as shown in Fig. 10, which is more effective than replacing the inclined reflecting surface by a cylindrical one. Because the light beam is strongly defocused in the azimuthal direction by the interface of the tube, immersed in Visipaque, the backpropagated light beam in the azimuthal direction is much smaller than required. Limited by this small spot size, the light beam cannot be focused back to the target focal point by a single cylindrical interface without magnifying the beam. With single cylindrical interface compensation, the difference in spot size will persist and manifest itself as a deviation not only in beam waist but also in working distance between the two directions.

Our simulation shows that the optimal correction is achieved with a radius of curvature $R_c = 0.75$ mm. After correction, the light beam in the azimuthal direction will focus at $z_{wx} = 1.89$ mm distance and form a beam waist $w_{0x} = 21.1$ μm. As shown in Table 3, although convergence in the azimuthal direction has been restored, effectively improving the beam, the beam remains astigmatic.

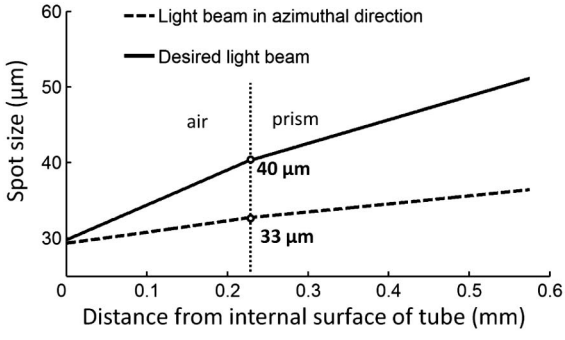

Fig. 9. Plot of spot size in Visipaque of the backpropagated light beam versus distance to internal surface of tube. The distance from the prism exit surface to the tube is 0.225 mm.

F. Compensation for Coronary Imaging by Index-Matching Flushing Liquid

Refractive index matching by flushing the catheter from inside with the proper index-matching liquid

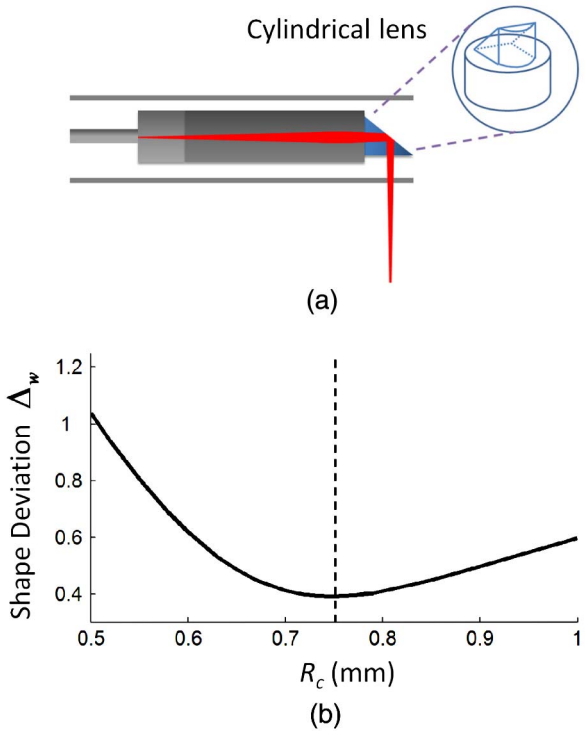

Fig. 10. (Color online) Schematic diagrams of simulation mode for a GRIN lens probe with a cylindrical lens mounted on the prism. The integral reaches its minimum value when the curvature radius is 0.75 mm. The parameters of GRIN lens and spacer are the same as Fig. 7. R_c: Curvature Radius.

Table 3. Characteristics of Light Beam after Compensation Showed as Spot Shapes in Visipaque[a]

		Emitting plane	Target focal plane	Rayleigh plane
Without compensation	z (mm)	0.50	1.89	3.39
	w_x at z (μm)	30.2	49.2	71.5
	w_y at z (μm)	28.3	20.8	29.4
	ellipticity	**1.07**	**2.37**	**2.43**
Curved interface	z (mm)	0.50	1.89	3.39
	w_x at z (μm)	23.4	22.8	36.1
	w_y at z (μm)	28.3	20.8	29.4
	ellipticity	**0.83**	**1.10**	**1.23**
Matching fluid	z (mm)	0.50	1.99	3.50
	w_x at z (μm)	28.7	19.2	30.4
	w_y at z (μm)	29.3	20.8	29.4
	ellipticity	**0.98**	**0.92**	**1.03**

[a]The Rayleigh plane is located at the Rayleigh distance in the y-direction.

can effectively neutralize the effect of the cylindrical tube by driving the C element of the ABCD matrix (1) towards 0.

$$\frac{n_2 - n_3}{R_1 n_2} + \frac{d(n_2 - n_3)(n_1 - n_2)}{R_1 R_2 n_2 n_3} + \frac{n_1 - n_2}{R_1 n_3} = 0. \quad (7)$$

However, the other elements of the ray transfer matrix are still different from the longitudinal direction, which will cause a slight astigmatism after compensation. When using Visipaque to displace blood, the refractive index of the matching fluid for optimal correction will be 1.465 by calculation. As the index of fluid is very close to Visipaque (1.45), it will be convenient to use Visipaque to flush the catheter as the matching fluid. The spot shape after compensation is also shown in Table 3.

4. Discussion

Endoscopic OCT has become a common diagnostic and research tool. Astigmatism of the imaging beam is a common side effect in sideview OCT endoscopes, which may degrade the image resolution and image contrast. Poor resolution in the longitudinal direction may not be apparent from the acquired data, because pullback OCT data are routinely undersampled in the pullback direction. In this paper, we present a quantitative analysis of the endoscope optics relating to the astigmatism, using fairly general assumptions about the catheter design. We also present a strategy for optimal compensation of the beam for specific imaging applications and geometries.

Particularly for short working distance probes working in air, the difference in optical characteristics between azimuthal and longitudinal directions can be well controlled by applying a thin-walled tube (relative to the tube diameter), made of low refractive index material. In this case the deviation from the design beam waist and working distance remain less than 10%.

Two current applications of catheter-based OCT do not operate in this limit, however. For long working distance probes, such as those used for imaging of the esophagus, and probes working in liquid, such as coronary imaging catheters, the astigmatism effect is so serious that extra compensation has to be designed. We implemented a simulation model for GRIN lens probes to evaluate the compensation methods. For catheters imaging the esophagus, with a long working distance of approximately 10 mm, our simulation demonstrates that a round spot shape can be restored by refocusing the light beam back to the focal point in the azimuthal direction with single cylindrical surface in the beam path. It is important that this surface be positioned in a plane transverse to the beam, where the uncorrected and ideal spot sizes are identical. In this case, a single curved surface suffices to adjust the beam convergence.

For uncompensated catheters working in a liquid environment, the beam actually becomes divergent in the azimuthal direction for $n_3 > 1.15$, which is practically for every fluid medium. In that case, compensation is more difficult than in air, as two curved surfaces are needed for full correction of the astigmatism. We demonstrated that convergence can be restored by means of a single cylindrical lens positioned as close as possible to the tube inner wall, but the beam remains astigmatic, with a deviation from the ideal spot size of 23%.

Another compensation method was also simulated by matching the refractive index inside the tube. Compared with the cylindrical interface method, the quality of spot profile along the line of sight is improved. For compatible catheter designs, fluid filling is an effective solution. Refractive index matching also has the engineering advantage in that it does not require accurately positioned curved surfaces. Drawbacks are the occasional occurrence of artifacts due to air bubbles in the flush liquid, and the requirement of an open hole in the catheter tip to maintain flush pressure inside the catheter tube during pullback. Blood may enter the catheter through the hole, which needs to be removed by flushing for repeat acquisitions.

The optimizations in this paper were performed by minimizing the integrated ratio w_x/w_y over the Rayleigh range. There are other performance measures which could be used, e.g., minimizing the difference between designed and realized working distance and beam waist. Such analysis could result in subtle differences in the end results, but the overall trend will be the same. It depends on the application requirements which measure is most appropriate.

5. Conclusion

We quantified the astigmatism in endoscopic OCT probes, which is introduced by the external tube and environment media, and analyzed compensation methods based on optics simulation. Based on the analysis of the probe optics, we presented optimal compensation schemes for common catheter types. A numerical analysis of minimizing the astigmatism such as performed here can facilitate the design and optimization of OCT imaging catheters for specific applications.

References

1. D. Huang, E. A. Swanson, C. P. Lin, J. S. Schuman, W. G. Stinson, W. Chang, M. R. Hee, T. Flotte, K. Gregory, C. A. Puliafito, and J. G. Fujimoto, "Optical coherence tomography," Science **254**, 1178–1181 (1991).
2. M. E. J. van Velthoven, D. J. Faber, F. D. Verbraak, T. G. van Leeuwen, and M. D. de Smet, "Recent developments in optical coherence tomography for imaging the retina," Prog. Retinal Eye Res. **26**, 57–77 (2007).
3. S. H. Yun, G. J. Tearney, B. J. Vakoc, M. Shishkov, W. Y. Oh, A. E. Desjardins, M. J. Suter, R. C. Chan, J. A. Evans, I.-K. Jang, N. S. Nishioka, J. F. de Boer, and B. E. Bouma, "Comprehensive volumetric optical microscopy in vivo," Nat. Med. **12**, 1429–1433 (2006).
4. H. L. Fu, Y. Leng, M. J. Cobb, K. Hsu, J. H. Hwang, and X. Li, "Flexible miniature compound lens design for high-resolution optical coherence tomography balloon imaging catheter," J. Biomed. Opt. **13**, 060502 (2008).
5. G. Lamouche, M. Dufour, M. Hewko, S. Vergnole, B. Gauthier, C. E. Bisaillon, J. P. Monchalin, and M. G. Sowa, "Intravascular optical coherence tomography on a beating heart model," J. Biomed. Opt. **15**, 046023 (2010).
6. X. Li, C. Chudoba, T. Ko, C. Pitris, and J. G. Fujimoto, "Imaging needle for optical coherence tomography," Opt. Lett. **25**, 1520–1522 (2000).
7. G. J. Tearney, S. A. Boppart, B. E. Bouma, M. E. Brezinski, N. J. Weissman, J. F. Southern, and J. G. Fujimoto, "Scanning single-mode fiber optic catheter-endoscope for optical coherence tomography," Opt. Lett. **21**, 543–545 (1996).
8. B. J. Vakoc, M. Shishko, S. H. Yun, W.-Y. Oh, M. J. Suter, A. E. Desjardins, J. A. Evans, N. S. Nishioka, G. J. Tearney, and B. E. Bouma, "Comprehensive esophageal microscopy by using optical frequency–domain imaging (with video)," Gastrointestinal endoscopy **65**, 898–905 (2007).
9. E. Regar, J. Ligthart, N. Bruining, and G. van Soest, "The diagnostic value of intracoronary optical coherence tomography," Herz **36**, 417–429 (2011).
10. F. J. van der Meer, D. J. Faber, I. Cilesiz, M. J. van Gemert, and T. G. van Leeuwen, "Temperature-dependent optical properties of individual vascular wall components measured by optical coherence tomography," J. Biomed. Opt. **11**, 041120 (2006).
11. G. J. Tearney, I. K. Jang, and B. E. Bouma, "Optical coherence tomography for imaging the vulnerable plaque," J. Biomed. Opt. **11**, 021002 (2006).
12. E. N. Brown, N. S. Burris, J. Gu, Z. N. Kon, P. Laird, S. Kallam, C. M. Tang, J. M. Schmitt, and R. S. Poston, "Thinking inside the graft: applications of optical coherence tomography in coronary artery bypass grafting," J. Biomed. Opt. **12**, 051704 (2007).
13. B. E. Bouma, G. J. Tearney, H. Yabushita, M. Shishkov, C. R. Kauffman, D. DeJoseph Gauthier, B. D. MacNeill, S. L. Houser, H. T. Aretz, E. F. Halpern, and I. K. Jang, "Evaluation of intracoronary stenting by intravascular optical coherence tomography," Heart **89**, 317–320 (2003).
14. P. Barlis, G. van Soest, P. W. Serruys, and E. Regar, "Intracoronary optical coherence tomography and the evaluation of stents," Expert Rev. Med. Devices **6**, 157–167 (2009).
15. G. van Soest, E. Regar, T. P. M. Goderie, N. Gonzalo, S. Koljenović, G. J. L. H. van Leenders, P. W. Serruys, and A. F. W. van der Steen, "Pitfalls in plaque characterization by OCT: image artifacts in native coronary arteries," J. Am. Coll. Cardiol. Img. **4**, 810–813 (2011).
16. G. van Soest, T. Goderie, E. Regar, S. Koljenovic, G. L. van Leenders, N. Gonzalo, S. van Noorden, T. Okamura, B. E. Bouma, G. J. Tearney, J. W. Oosterhuis, P. W. Serruys, and A. F. van der Steen, "Atherosclerotic tissue characterization in vivo by optical coherence tomography attenuation imaging," J. Biomed. Opt. **15**, 011105 (2010).
17. M. L. Dufour, C.-E. Bisaillon, G. Lamouche, S. Vergnole, M. Hewko, F. D'Amours, C. Padioleau, and M. Sowa, "Tools for experimental characterization of the non-uniform rotational distortion in intravascular OCT probes," Proc. SPIE **7883**, 788339 (2011).
18. A. R. Tumlinson, L. P. Hariri, U. Utzinger, and J. K. Barton, "Miniature endoscope for simultaneous optical coherence tomography and laser-induced fluorescence measurement," Appl. Opt. **43**, 113–121 (2004).
19. P. Meemon, K. S. Lee, S. Murali, and J. Rolland, "Optical design of a dynamic focus catheter for high-resolution endoscopic optical coherence tomography," Appl. Opt. **47**, 2452–2457 (2008).
20. J. Xi, L. Huo, Y. Wu, M. J. Cobb, J. H. Hwang, and X. Li, "High-resolution OCT balloon imaging catheter with astigmatism correction," Opt. Lett. **34**, 1943–1945 (2009).
21. W. Kang, H. Wang, Y. Pan, M. W. Jenkins, G. A. Isenberg, A. Chak, M. Atkinson, D. Agrawal, Z. Hu, and A. M. Rollins, "Endoscopically guided spectral-domain OCT with double-balloon catheters," Opt. Express **18**, 17364–17372 (2010).
22. W. Drexler and J. G. Fujimoto, *Optical Coherence Tomography: Technology and Applications* (Springer, 2008), pp. 397–400.
23. E. Swanson, C. L. Petersen, E. McNamaram, R. B. Lamport, and D. L. Kelly, "Ultra-small optical probes, imaging optics, and methods for using same," U.S. Patent 6445939 (3 September 2002).
24. Z. Yaqoob, J. Wu, E. J. McDowell, X. Heng, and C. Yang, "Methods and application areas of endoscopic optical coherence tomography," J. Biomed. Opt. **11**, 063001 (2006).
25. Y. Mao, S. Chang, S. Sherif, and C. Flueraru, "Graded-index fiber lens proposed for ultrasmall probes used in biomedical imaging," Appl. Opt. **46**, 5887–5894 (2007).
26. W. Jung, W. Benalcazar, A. Ahmad, U. Sharma, H. Tu, and S. A. Boppart, "Numerical analysis of gradient index lens-based optical coherence tomography imaging probes," J. Biomed. Opt. **15**, 066027 (2010).
27. W. T. Silfvast, *Laser Fundamentals* (Cambridge University, 2003), pp. 402–432.
28. C. Gomez-Reino, M. V. Perez, and C. Bao, *Gradient-Index Optics* (Springer, 2002).
29. C. W. Reno, "Laser astigmatism compensation," U.S. Patent 5239414 (24 August 1993).